PNAS PLUS

Creatine maintains intestinal homeostasis and protects against colitis

Emre Turer[a,b], William McAlpine[a], Kuan-wen Wang[a], Tianshi Lu[a], Xiaohong Li[a], Miao Tang[a], Xiaoming Zhan[a], Tao Wang[a,c], Xiaowei Zhan[a,c], Chun-Hui Bu[a], Anne R. Murray[a], and Bruce Beutler[a,1]

[a]Center for the Genetics of Host Defense, University of Texas Southwestern Medical Center, Dallas, TX 75390-8505; [b]Department of Internal Medicine, Division of Gastroenterology, University of Texas Southwestern Medical Center, Dallas, TX 75390-8505; and [c]Quantitative Biomedical Research Center, Department of Clinical Science, University of Texas Southwestern Medical Center, Dallas, TX 75390

Contributed by Bruce Beutler, December 28, 2016 (sent for review October 12, 2016; reviewed by Ralph S. Baric and Michael J. Gale Jr.)

Creatine, a nitrogenous organic acid, replenishes cytoplasmic ATP at the expense of mitochondrial ATP via the phosphocreatine shuttle. Creatine levels are maintained by diet and endogenous synthesis from arginine and glycine. Glycine amidinotransferase (GATM) catalyzes the rate-limiting step of creatine biosynthesis: the transfer of an amidino group from arginine to glycine to form ornithine and guanidinoacetate. We screened 36,530 third-generation germline mutant mice derived from *N*-ethyl-*N*-nitrosourea–mutagenized grandsires for intestinal homeostasis abnormalities after oral administration of dextran sodium sulfate (DSS). Among 27 colitis susceptibility phenotypes identified and mapped, one was strongly correlated with a missense mutation in *Gatm* in a recessive model of inheritance, and causation was confirmed by CRISPR/Cas9 gene targeting. Supplementation of homozygous *Gatm* mutants with exogenous creatine ameliorated the colitis phenotype. CRISPR/Cas9-targeted ($Gatm^{c/c}$) mice displayed a normal peripheral immune response and immune cell homeostasis. However, the intestinal epithelium of the $Gatm^{c/c}$ mice displayed increased cell death and decreased proliferation during DSS treatment. In addition, $Gatm^{c/c}$ colonocytes showed increased metabolic stress in response to DSS with higher levels of phospho-AMPK and lower levels of phosphorylation of mammalian target of rapamycin (phospho-mTOR). These findings establish an in vivo requirement for rapid replenishment of cytoplasmic ATP within colonic epithelial cells in the maintenance of the mucosal barrier after injury.

mTOR | *N*-ethyl-*N*-nitrosourea | inflammatory bowel disease | glycine amidinotransferase

In the intestinal tract, the balance between the ability to respond to pathogens and tolerance to normal commensal bacteria must be maintained. This balance is dependent on intact mucosal barrier function as well as regulation of both the innate and adaptive immune responses. Perturbations in this balance can result in inflammatory bowel disease (IBD) (1–3). Many of the molecules needed to enforce homeostasis remain unidentified.

Orally administered dextran sodium sulfate (DSS) can damage the intestinal mucosa and disrupt intestinal homeostasis in the mouse. Restoration of intestinal homeostasis requires several factors, including epithelial cell proliferation and differentiation, vesicle trafficking, protein secretion, integrity of the unfolded protein response pathways, and immune signaling (4–8). The essential molecular components required for a physiological response to the damage caused by DSS can be revealed by random germline mutagenesis (4). Accordingly, we carried out a forward genetic screen of *N*-ethyl-*N*-nitrosourea (ENU)-induced mutant mice exposed to DSS to identify genes involved in intestinal homeostasis. One of the candidate genes, *Gatm*, was validated using CRISPR/Cas9 targeting. *Gatm* encodes glycine amidinotransferase (GATM), which catalyzes the rate-limiting step of creatine biosynthesis, catalyzing the transfer of an amidino group from arginine to glycine to form ornithine and guanidinoacetate. The identification of the mutation in *Gatm* demonstrates that abnormal cellular energy metabolism can promote the induction of colitis.

Results

DSS Screening of ENU-Induced Mutant Mice. We designed a screen to identify genes required for intestinal homeostasis. Third-generation (G3) mutant mice were exposed to 1.5% (wt/vol) DSS in their drinking water for 7 d and then placed on drinking water without DSS for an additional 3 d. Body weights of the G3 mice were assessed at day 0, 7, and 10. A total of 36,530 G3 mice from 1,253 pedigrees were screened for phenovariance in the DSS screen (Table 1). These pedigrees were a repository of 66,652 validated mutations in 17,853 genes; 47,664 mutations in 14,126 genes were transmitted to homozygosity three or more times, and examined for phenotypic effects. Among the 47,664 mutations transmitted to homozygosity three or more times, 2,738 mutations in 2,147 genes produced overt null effects (premature stop codons or critical splice junction errors), whereas 17,516 mutations in 8,132 genes were predicted to be "probably damaging" by Polymorphism Phenotyping v2 (PolyPhen-2) with a score of 0.95 or greater (9).

During the course of the DSS screen, linkage mapping identified putative causative mutations in 27 pedigrees (Table 2). Twenty-three pedigrees contained at least two homozygous variant mice that exhibited at least 10% more weight loss than wild-type or heterozygous littermate controls, resulting in *P* values for linkage of less than 10^{-5} with Bonferroni correction. A number of genes known to cause DSS sensitivity were mapped by this method, including *Yap1*, *Ern2*, and *Klf5* (10–12). One gene, *Smcr8*, was mapped in two separate pedigrees with different alleles, indicating a high likelihood of validation as a causative mutation. *Lrba*, a gene known to cause common variable immunodeficiency with autoimmunity-8 (CVID8) [Online Mendelian Inheritance in Man (OMIM) ID no. 614700] and IBD in humans (13–15), was also mapped by this method, validating our screen as a means to identify human disease genes and components

Significance

The present study used a forward genetic approach to identify new causative mutations in an environmentally sensitized screen for colitis. A candidate mutation in *Gatm*, verified by CRISPR/Cas9 targeting, demonstrated the need for rapid replenishment of cytoplasmic ATP within colonic epithelial cells to restore barrier integrity. This environmentally specified requirement for energy to avert colitis suggests a new category of mutations with the potential to cause inflammatory bowel disease.

Author contributions: E.T. and B.B. designed research; E.T., W.M., K.-w.W., and T.L. performed research; X.L., M.T., Xiaoming Zhan, T.W., Xiaowei Zhan, and C.-H.B. contributed new reagents/analytic tools; E.T., Xiaowei Zhan, and B.B. analyzed data; and E.T., A.R.M., and B.B. wrote the paper.

Reviewers: R.S.B., University of North Carolina at Chapel Hill; and M.J.G., University of Washington School of Medicine.

The authors declare no conflict of interest.

[1]To whom correspondence should be addressed. Email: bruce.beutler@utsouthwestern.edu.

This article contains supporting information online at www.pnas.org/lookup/suppl/doi:10.1073/pnas.1621400114/-/DCSupplemental.

Table 1. Saturation to homozygosity

Type of mutation	No. of hits	Pedigrees	G3 mice	Genes	Alleles	Saturation, %
All mutations	≥0	1,253	36,530	17,853	66,652	71.48
	≥1	1,245	33,611	16,418	50,118	65.73
	≥2	1,245	33,600	15,310	49,011	61.3
	≥3	1,245	33,576	14,126	47,664	56.56
Probably null* or probably damaging**	≥0	1,253	36,530	12,609	27,798	50.48
	≥1	1,245	29,395	10,624	20,130	42.54
	≥2	1,245	29,274	9,398	18,905	37.63
	≥3	1,245	29,019	8,132	17,516	32.56
Probably null	≥0	1,236	36,031	4,838	6,237	19.37
	≥1	1,167	12,622	3,293	3,894	13.18
	≥2	1,126	12,289	2,717	3,318	10.88
	≥3	1,065	11,592	2,147	2,722	8.6

*Probably null: nonsense, makesense, splicing errors, frameshift indels, start loss, or start gain mutations; designation not provided by PolyPhen-2.
**Probably damaging: PolyPhen-2 score of 0.95–1.0.

of IBD pathogenesis. Mutations in four pedigrees conferred resistance to DSS, mapping to mutations in *Gpat2*, *Hesx1*, *Lck*, and *Zfp219* (Table 2). Unexpectedly, a large number of metabolism- and mitochondria-associated genes were mapped, including *Gatm*, *Mtif3*, and *Glyat.*

Recessive DSS Susceptibility Phenotype Associated with a Missense Mutation in Gatm. A DSS susceptibility mutant, named *mrbig* ($Gatm^{mb/mb}$), exhibited weight loss at day 7 in the DSS screen (Fig. 1*A*). The *mrbig* phenotype was mapped using a recessive model of inheritance ($P = 5.562 \times 10^{-9}$) to a missense mutation in *Gatm* (Chr2:122,600,744, GRCm38; Fig. 1*B*). A semidominant effect was also observed, but the mutation is preponderantly recessive. The *mrbig* mutation results in an aspartic acid-to-glycine substitution at amino acid 254 in the GATM protein (Fig. 1 *C*–*E*). Asp254 is one of the three key enzymatic amino acids within the catalytic triad (Fig. 1*D*) (16).

$Gatm^{mb/mb}$ mice showed severe muscle wasting similar to *Gatm*-deficient ($Gatm^{-/-}$) mice (17). Moreover, $Gatm^{mb/mb}$ mice exhibited creatine deficiency in the intestinal epithelium (Fig. 1*F*). As with $Gatm^{-/-}$ mice, the muscle-wasting phenotype was reversed after exogenous oral creatine supplementation (Fig. 1*G*).

A Western blot of colon extracts from the $Gatm^{mb/mb}$ mice showed normal levels of GATM protein (Fig. 1*H*), demonstrating that this mutation does not affect protein stability, but more likely enzymatic function.

DSS Treatment of $Gatm^{mb/mb}$ Mice Causes Colitis. The $Gatm^{mb/mb}$ mice exhibited high mortality rates (87%, $n = 8$) by day 14 post-DSS treatment compared with heterozygous ($Gatm^{mb/+}$; 14%, $n = 14$) and wild-type ($Gatm^{+/+}$; 0%, $n = 8$) littermates (Fig. 2*A*). Furthermore, the $Gatm^{mb/mb}$ and $Gatm^{mb/+}$ mice exhibited diarrhea and rectal bleeding after DSS treatment. Macroscopic examination of colons from untreated $Gatm^{mb/mb}$ mice showed normal length (Fig. 2*B*, *Lower*). After DSS exposure, the colons of $Gatm^{mb/mb}$ mice showed shortening compared with those of DSS-treated wild-type mice (Fig. 2*B*). Histologic examination of colons from DSS-treated $Gatm^{mb/mb}$ mice demonstrated loss of crypt architecture, a denuded epithelial layer, and prominent inflammatory infiltrates (Fig. 2*C*). A decrease in epithelial cell viability should increase the translocation of insoluble material from the lumen into the systemic circulation. To investigate this process in vivo, $Gatm^{mb/mb}$ mice were gavaged with nonabsorbable FITC–dextran. The $Gatm^{mb/mb}$ mice showed increased permeability to the nonabsorbable dextran (Fig. 2*D*), demonstrating that creatine is necessary for maintenance of epithelial barrier function in vivo.

$Gatm^{mb/mb}$ mice supplemented with creatine [1% (wt/vol) in drinking water] and treated with DSS exhibited similar levels of weight loss and colonic shortening as wild-type mice after DSS treatment (Fig. 2 *E* and *F*, respectively). Notably, creatine [1% (wt/vol)] did not ameliorate colitis in wild-type mice given colitis-inducing doses of DSS (Fig. 2*G*). Taken together, a basal level of creatine is necessary to maintain energy homeostasis in the colon, but supraphysiological levels do not provide additional benefit.

CRISPR/Cas9-Targeted Mice Validate That the *Gatm* Mutation Is Causative of the *mrbig* Phenotype. To determine whether the observed *Gatm* mutation was causative of the *mrbig* phenotype, CRISPR/Cas9-mediated targeting was used to generate a frame-shift

Table 2. Candidate mutations in the DSS colitis screen

Gene	Mutation	Inheritance	Ref	Het	Var	*P*
1700112E06Rik	Y13*	Recessive	20	24	5	1.22E-08
Cars	E430G	Recessive	9	14	2	6.17E-09
Col3a1	Splice donor	Recessive	19	17	2	1.30E-06
Col4a1	G1341V	Dominant	7	9	0	1.34E-05
Degs2	N189D	Recessive	8	9	6	4.40E-05
Ern2	Splice donor	Recessive	12	20	10	2.20E-10
Gatm	D254G	Recessive	8	7	6	5.56E-09
Glyat	V247F	Recessive	10	7	3	1.79E-06
Gpat2†	V75M	Recessive	11	16	10	1.84E-05
Hesx1†	W45R	Dominant	6	9	2	4.51E-06
Hgf	H649L	Recessive	6	10	2	8.11E-09
Hr	L1091P	Recessive	5	15	5	1.91E-07
Hsd11b2	V270E	Recessive	2	6	4	2.44E-09
Klf5	R360C	Additive	24	29	5	1.78E-07
Lars2	I305N	Recessive	3	10	4	6.09E-08
Lck†	E299G	Recessive	2	9	6	2.07E-06
Liph	I204N	Recessive	15	25	5	6.12E-07
Lrba	Q1292*	Recessive	16	11	5	2.98E-06
Mnd1	C62F	Recessive	18	14	3	4.55E-05
Mtif3	R249S	Recessive	8	7	2	8.10E-06
Myo1d	L972P	Recessive	12	19	10	1.47E-09
Nlrp4d	K762N	Recessive	5	19	4	1.88E-05
Rnps1	F181I	Recessive	27	23	4	1.41E-06
Smcr8	I2T	Recessive	10	13	3	6.41E-08
Smcr8	M1V	Recessive	6	13	4	7.71E-06
Yap1	G36D	Additive	4	7	8	3.39E-05
Zfp219†	T595S	Dominant	9	16	3	5.01E-06

Ref, wild type; Het, heterozygous; Var, homozygous variant.
*Stop codon.
†Genes conferred resistance to DSS-induced colitis.

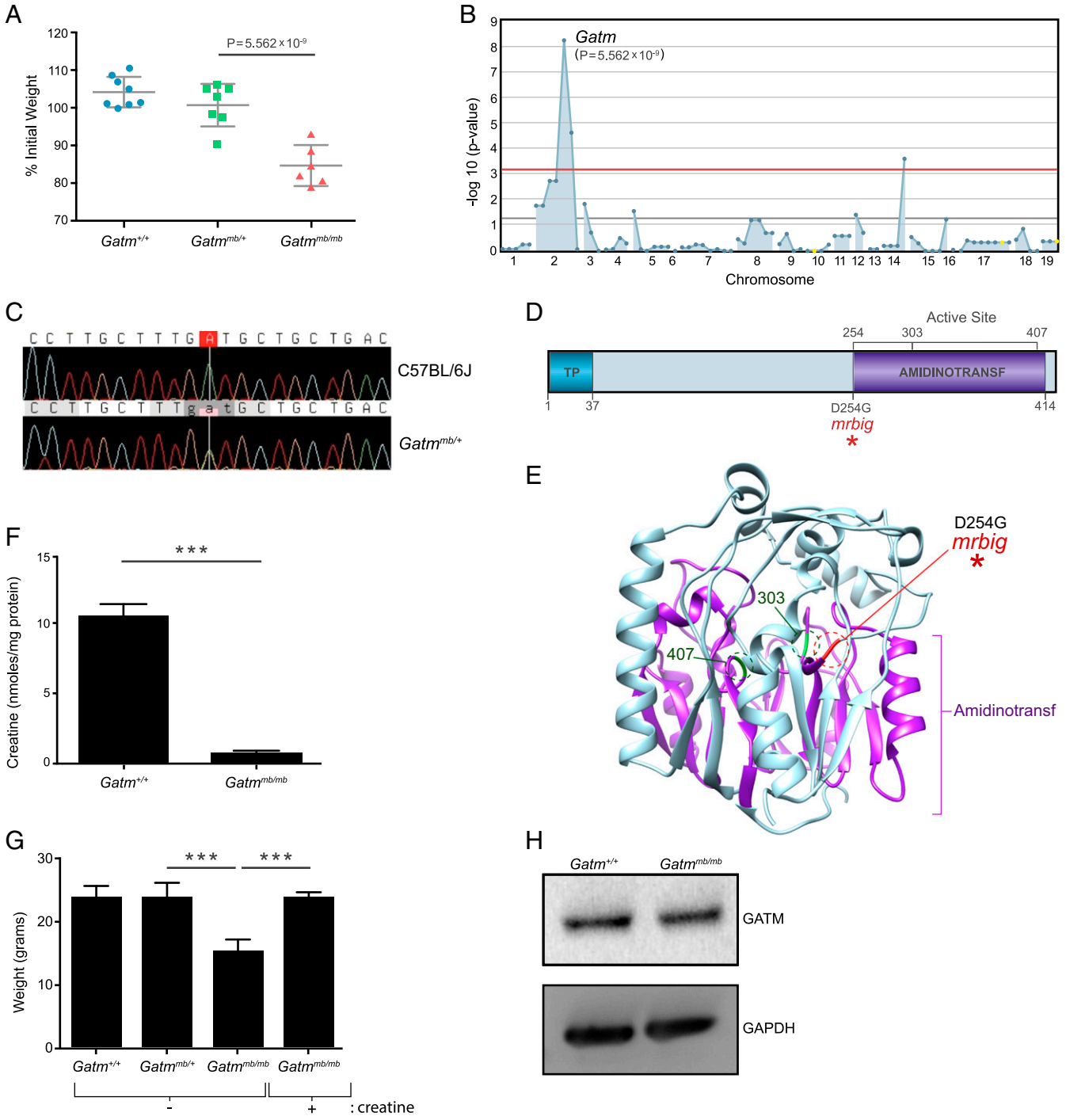

Fig. 1. Mapping of the *mrbig* mutation in *Gatm*. (*A*) Weight loss analysis of the *mrbig* pedigree in response to 1.5% DSS. REF, $Gatm^{+/+}$ ($n = 8$); HET, $Gatm^{mb/+}$ ($n = 7$); VAR, $Gatm^{mb/mb}$ ($n = 6$). Data points represent individual mice; mean and SD are indicated. (*B*) Manhattan plot showing −log10 *P* values (*y* axis) plotted against the chromosome positions of 77 mutations (*x* axis) identified in the G1 male mouse of pedigree R0046. Linkage between the *mrbig* phenotype and the *Gatm* mutation using a recessive model of inheritance. Horizontal pink and red lines represent thresholds of $P = 0.05$, and the threshold for $P = 0.05$ after applying Bonferroni correction, respectively. (*C*) DNA chromatogram trace showing the *Gatm* point mutation. (*D*) Protein domain diagram and (*E*) crystal structure (PDB ID code 1JDW) of GATM with the *mrbig* mutation indicated. Amidinotransf, glycine amidinotransferase domain; TP, transit peptide. (*F*) Creatine concentration in $Gatm^{mb/mb}$ ($n = 3$) and littermate control ($Gatm^{+/+}$, $n = 4$) colonic epithelial cells. ***$P < 0.0001$. (*G*) Creatine supplementation restored the body weights in male $Gatm^{mb/mb}$ mice ($n = 3$; ***$P < 0.0001$). (*H*) GATM protein levels in colonic tissue from $Gatm^{+/+}$ and $Gatm^{mb/mb}$ mice. Blot is representative of four individual experiments. (*A*, *F*, and *G*) *P* values were calculated by Student's *t* test. (*F* and *G*) Bars indicate mean ± SD.

mutation at the *Gatm* transcription start site. CRISPR/Cas9-targeted ($Gatm^{c/c}$) colonic epithelial cells were deficient in intracellular creatine compared with wild-type cells, and mice showed shortened colon length after DSS treatment (Fig. S1). During the course of DSS treatment, compound heterozygotes ($Gatm^{mb/c}$) showed weight loss as early as day 5, and more than a 20% weight loss with respect to initial weight by day 7 (Fig. 3*A*). Furthermore, the $Gatm^{mb/c}$ mice had colonic shortening as well as

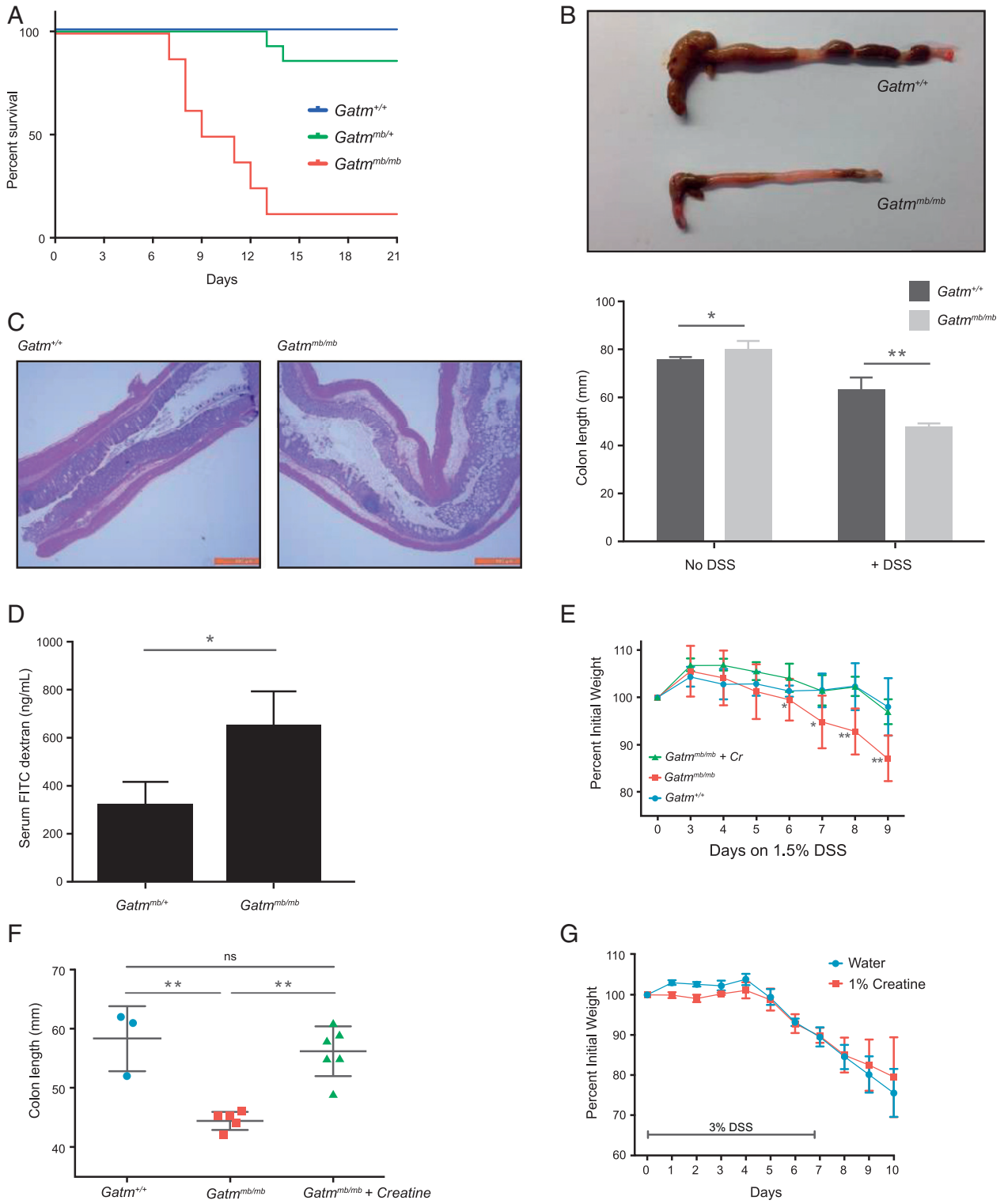

Fig. 2. *Mrbig* mice exhibit characteristic symptoms of colitis. (*A*) Kaplan–Meier survival plot showing that $Gatm^{mb/mb}$ mice ($n = 8$) exhibit increased mortality after DSS compared with littermate controls [$Gatm^{+/+}$ ($n = 8$) and $Gatm^{mb/+}$ ($n = 14$)]. (*B*) Colons of mice exposed to 10-d DSS treatment exhibited shortening ($n = 3$ per genotype). Representative colons (*Upper*; after DSS treatment) and colon length (*Lower*). Bars indicate mean ± SD; $^{**}P < 0.01$. (*C*) Histologic examination of $Gatm^{mb/mb}$ colons after 7 d of DSS treatment (10× magnification). (*D*) Intestinal permeability was determined by serum concentration 4 h after FITC–dextran gavage. $Gatm^{+/+}$ ($n = 3$) and $Gatm^{mb/mb}$ ($n = 4$) littermates were analyzed after 4 d of DSS treatment. Bars indicate mean ± SD; $^{*}P < 0.05$. (*E*) Supplementation of $Gatm^{mb/mb}$ mice with exogenous creatine [1% (wt/vol) in drinking water] during DSS treatment rescues the DSS-induced weight loss. Data points indicate mean ± SD; $^{*}P < 0.05$, $^{**}P < 0.005$ (vs. $Gatm^{mb/mb}$ group). $Gatm^{+/+}$ ($n = 3$), $Gatm^{mb/mb}$ ($n = 5$), and $Gatm^{mb/mb}$ plus creatine supplementation ($n = 6$). (*F*) Colon length was restored in $Gatm^{mb/mb}$ mice after creatine supplementation. $Gatm^{+/+}$ ($n = 3$), $Gatm^{mb/mb}$ without creatine supplementation ($n = 5$), and $Gatm^{mb/mb}$ with creatine supplementation ($n = 6$) littermates were analyzed on day 10 of treatment. Data points represent individual mice; mean and SD are indicated. ns, not significant; $^{**}P < 0.01$. (*G*) Supplementation of $Gatm^{+/+}$ mice with a high dose [1% (wt/vol)] of creatine during high-dose (3%) DSS treatment does not rescue weight loss. Data from mice treated with water alone ($n = 4$) or 1% creatine ($n = 4$) are shown. Data points indicate mean ± SD. (*B*, *D*, *E*, and *F*) *P* values were calculated by Student's *t* test.

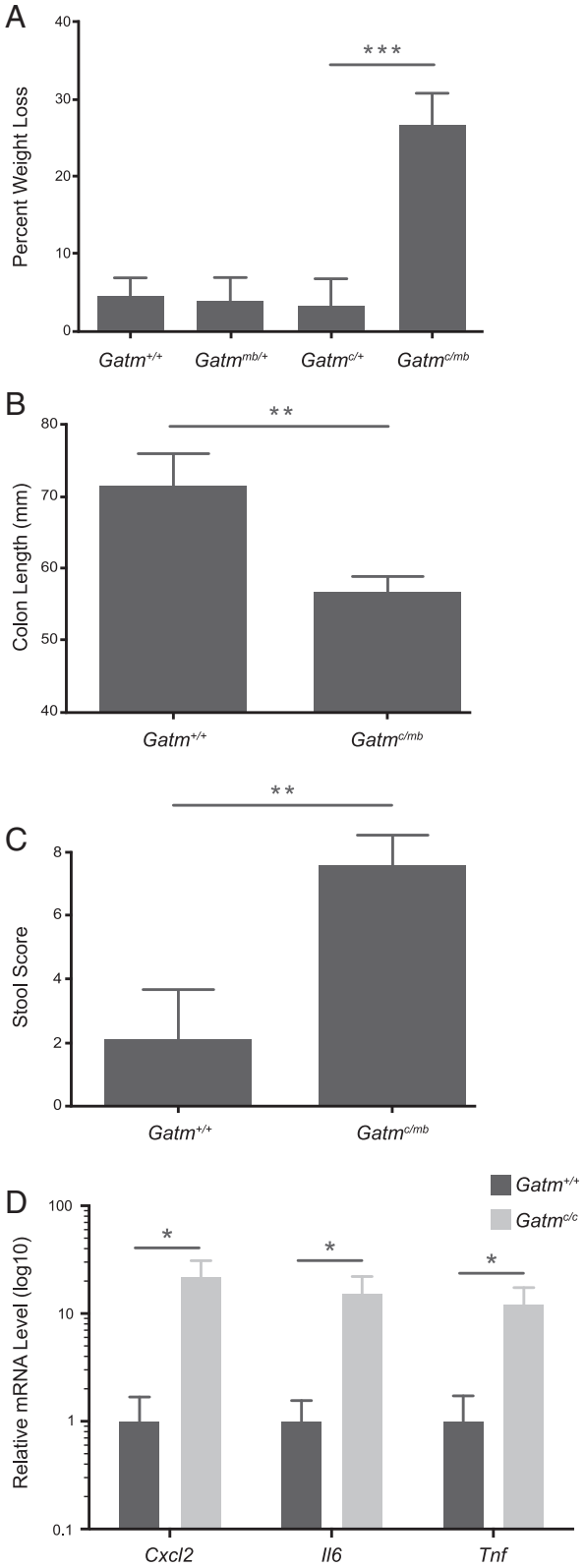

Fig. 3. Validation that a mutation in *Gatm* causes the *mrbig* phenotype. (*A*) Weight loss analysis of the $Gatm^{mb/c}$ mice in response to 1.5% DSS. $Gatm^{+/+}$ ($n = 3$), $Gatm^{mb/+}$ ($n = 4$), $Gatm^{c/+}$ ($n = 5$), and $Gatm^{mb/c}$ ($n = 5$) mice were analyzed on day 8 of treatment. ***$P < 0.001$. (*B*) Colons of $Gatm^{mb/c}$ mice exposed to DSS on day 8 of treatment exhibited shortening ($n = 5$). $Gatm^{+/+}$ ($n = 3$) mice were also analyzed. **$P < 0.01$. (*C*) Stool scores in $Gatm^{mb/c}$ mice 7 d after administration of 1.5% DSS. $Gatm^{+/+}$ ($n = 3$) and $Gatm^{mb/c}$ ($n = 5$) mice were analyzed. **$P < 0.01$. (*D*) Relative mRNA expression levels of inflammatory cytokines *Cxcl2*, *Il6*, and *Tnf* in the distal colon of $Gatm^{+/+}$ ($n = 3$) and $Gatm^{c/c}$ ($n = 3$) mice after 6 d of 1.5% DSS. Experiment was repeated three times; *$P < 0.05$. (*A–D*) *P* values were calculated by Student's *t* test; bars indicate mean ± SD.

diarrhea and rectal bleeding after DSS treatment (Fig. 3 *B* and *C*, respectively). Additionally, the expression of proinflammatory genes, including *Cxcl2*, *Tnf*, and *Il6*, were increased in the colons from homozygous $Gatm^{c/c}$ mice compared with that in wild-type mice (Fig. 3*D*). $Gatm^{c/c}$ mice were hypersensitive to rectally administered trinitrobenzenesulfonic acid, demonstrating shortened colonic length (Fig. S2). Taken together, the findings from the $Gatm^{mb/c}$ mice validates that the *Gatm* mutation causes the DSS-induced colitis phenotype observed in the $Gatm^{mb/mb}$ mice.

$Gatm^{c/c}$ Mice Have Normal Peripheral Immune Responses. Creatine has been implicated in a number of immune activation pathways (18). To assess a role for GATM and creatine in immune cell homeostasis, flow cytometric analysis was performed on peripheral blood from $Gatm^{c/c}$ mice. The relative proportions of B cells, T cells, macrophages, natural killer cells, and granulocytes were comparable between the $Gatm^{c/c}$ and wild-type mice (Fig. 4*A*). $Gatm^{c/c}$ mice were immunized with the T-independent antigen NP-Ficoll or a recombinant Semliki Forest virus vector encoding the model antigen β-galactosidase (rSFV-β-gal), a T-dependent antigen. The antibody titers in response to NP-Ficoll and rSFV–β-gal immunization were comparable between $Gatm^{c/c}$ and wild-type mice (Fig. 4 *B* and *C*, respectively), demonstrating that antibody production, T helper function, and antigen presentation in a creatine-deficient state were intact. These findings suggest that the increased colitis susceptibility in the $Gatm^{mb/mb}$ mice is unlikely to be intrinsic to immune cells.

Increased Cell Death and Decreased Proliferation in $Gatm^{c/c}$ Epithelium. Creatine has a protective role against metabolic and hypoxic cell death in vitro (19–21). To examine cell death in vivo, colons from $Gatm^{c/c}$ and wild-type mice were examined for cell death by TUNEL staining on the fourth day of DSS treatment. In the $Gatm^{c/c}$ mice, numerous TUNEL-positive cells were observed within the colonic crypts (Fig. 5*A*). In contrast, distal colons from wild-type mice showed low levels of TUNEL-positive staining. Excessive cell death in the $Gatm^{c/c}$ colon occurred in tissue sections containing large amounts of infiltrating cells as well as those with an intact epithelial layer. $Gatm^{mb/mb}$ colons displayed a similar excessive cell death response when challenged with DSS (Fig. S3). Together, these data show that creatine is necessary for maintaining epithelial cell viability under inflammatory conditions.

A key response to DSS-induced damage is increased cell proliferation in colonic crypts. In the absence of a proliferative response, colonocytes fail to regenerate, resulting in increased permeability and subsequent inflammation. To examine the proliferative index in a creatine-deficient state, $Gatm^{c/c}$ mice were injected with the DNA-nucleoside analog 5-ethynyl-2′-deoxyuridine (EdU) on day 4 of DSS treatment. $Gatm^{c/c}$ colons showed reduced cell proliferation in comparison with colons from wild-type mice (Fig. 5*B*), indicating that a proliferative defect contributes to DSS susceptibility in creatine-deficient mice.

$Gatm^{c/c}$ Colonocytes Have Abnormal Cellular Metabolic Responses. AMPK, a key sensor of intracellular energy, regulates cellular metabolism, proliferation, and cell death pathways. AMPK opposes the activation of the mammalian target of rapamycin (mTOR) signaling pathway and is up-regulated in skeletal muscle of creatine-deficient animals (22). In colonic epithelial cells, activation of AMPK leads to increased susceptibility to apoptotic stimuli (23). We examined whether DSS-induced colitis induces AMPK phosphorylation in isolated colonic epithelium from

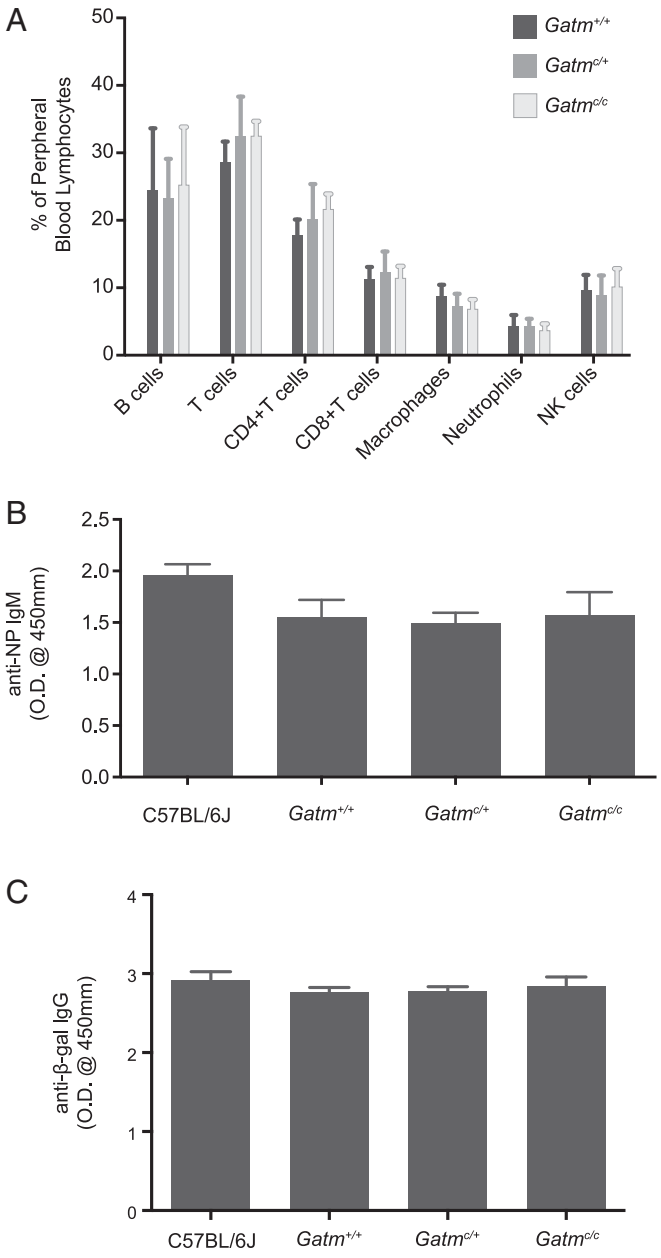

Fig. 4. The $Gatm^{c/c}$ mice exhibit normal peripheral immune homeostasis and responses. (*A*) Flow cytometry analysis of peripheral blood B cells ($B220^+$), $CD4^+$ T cells ($CD3^+$ $CD4^+$), $CD8^+$ T cells ($CD3^+CD8^+$), macrophages ($F480^+$), neutrophils ($CD11b^+F480^-$) and NK cells ($NK1.1^+CD3^-$) in $Gatm^{+/+}$ ($n = 6$), $Gatm^{c/+}$ ($n = 9$), and $Gatm^{c/c}$ ($n = 5$) mice. (*B* and *C*) Serum NP-specific IgM (*B*) and β-gal–specific IgG (*C*) measured by ELISA in $Gatm^{+/+}$ ($n = 6$), $Gatm^{c/+}$ ($n = 9$), and $Gatm^{c/c}$ ($n = 5$) mice immunized 5 or 14 d before with NP-Ficoll and rSFV–β-gal, respectively. Bars indicate mean ± SD. Differences between genotypes were not found to be statistically significant ($P > 0.05$).

$Gatm^{c/c}$ mice. AMPK phosphorylation was increased in $Gatm^{c/c}$ colonic epithelium in response to DSS, demonstrating a relative energy deficiency within the cells (Fig. 5*C*). Up-regulation of the mTOR pathway aids in epithelial regeneration in response to DSS and other colitis-inducing stimuli (24, 25). However, in DSS-treated $Gatm^{c/c}$ mice there was a reduction in mTOR phosphorylation compared with DSS-treated wild-type mice (Fig. 5*D*). There was no reduction in mitochondrial number at day 3 in DSS treatment. Additionally, mitochondrial function was unperturbed early in DSS treatment (day 3), indicating a normal production of ATP through oxidative phosphorylation (Fig. S4). Therefore, we propose that the failure to regenerate the colonic epithelium in $Gatm^{mb/mb}$ and $Gatm^{c/c}$ mice is due to an acute loss in ATP-dependent intracellular signaling.

Discussion

In the present study, we have established a DSS-induced colitis screen using ENU-mutagenized mice to identify monogenic causes of altered intestinal homeostasis. A minimum of 8.6% and a maximum of 32.6% of genes were damaged or destroyed by ENU-induced mutations and tested in the homozygous state three times or more. Although not all genes identified in the DSS-induced colitis screen have been validated by CRISPR/Cas9 targeting, the identification of a number of previously described colitis susceptibility genes indicates that this screen is a reliable method to detect genetic causes of DSS susceptibility. Using this unbiased approach, we have found a number of genes with key cellular functions, including cellular metabolism. For example, delta(4)-desaturase, sphingolipid 2 (Degs2) regulates biosynthesis of the lipid ceramide, which is a regulator of whole organism metabolism (26–28). In addition, mitochondrial translation initiation factor 3 (Mtif3), glycine *N*-acyltransferase (Glyat), and glycerol-3-phosphate acyltransferase-2 (Gpat2) are localized to the mitochondria and presumably exert their functions there (29–31).

During inflammation, the intestinal epithelium exhibits increased hypoxic stress, which requires metabolic alterations to maintain the barrier function of this tissue (32–34). DSS is a metabolic stressor of epithelial cells. Creatine may provide an energy buffer in the face of acutely increased energy requirements; it also facilitates the transfer of high-energy phosphate from the mitochondria to the cytosol via the phosphocreatine shuttle, which may be important during the regeneration of the mucosal barrier. We have shown that a missense mutation in the catalytic site of GATM causes impairment of epithelial integrity and an increased susceptibility to DSS-induced colitis. To date, no association between human IBD and SNPs of *GATM* or other creatine pathway genes has been identified, although creatine kinase levels have been found to be low in chronic IBD patients (35, 36). The loss of creatine in vivo leads to increased epithelial cell death and colitis, directly linking energy metabolism to intestinal homeostasis. This unique mutation affects energy metabolism in the colon and subsequently leads to colitis susceptibility. During inflammatory stress, creatine serves as a protective factor to prevent cell death and maintain proliferative responses. The creatine pathway reflects a critical protective mechanism by which cells are able to survive both acute and chronic metabolic deficiencies.

Creatine is a protective factor during hypoxia that maintains an adequate ATP pool (37). The role for creatine in intestinal homeostasis is an evolving field of study. Many of the genes in the creatine utilization pathway, including the creatine kinases, are metabolically regulated and are needed to maintain epithelial barrier integrity in vitro (35). We demonstrated the effects of loss of GATM function on intestinal homeostasis in vivo. Our data show that loss of GATM function leads to increased susceptibility to colitis as well as a reduction in mTOR-associated signaling. The mTOR pathway has been shown to be critical in epithelial regeneration in response to colitis (24, 25). Additionally, it is well established that AMPK activation inhibits proliferation as well as increases colonic epithelium cell death susceptibility in vitro (23, 38–40). Although some of creatine's effects are AMPK-dependent, the link between creatine and colitis is less established due to the profound and diverse effects of AMPK signaling, including its antiinflammatory functions within macrophage populations (41–43). Tissue-specific disruption of AMPK signaling would therefore be needed to definitively establish the link between creatine and AMPK signaling in colitis. mTOR, which is directly regulated by AMPK, has been investigated in a tissue-specific manner and is essential for epithelial regeneration in response to colitis similar to *Gatm*-deficient animals (25).

We have identified an essential and nonredundant role for GATM and creatine metabolism in epithelial cell barrier function and intestinal homeostasis maintenance in vivo. This study highlights the importance of energy metabolism and balance in maintaining the epithelial barrier during times of acute injury. In cases of aberrant energy metabolism, increased epithelial cell death and decreased proliferative responses occur. Although this study focused on intestinal homeostasis, creatine may play a role in tissue barrier maintenance at other epithelial surfaces, for example in the lung. Interestingly, creatine supplementation has been implicated in excessive lung allergic responses and further investigation seems warranted to determine whether loss of creatine leads to a loss of type 2 immune responses (44). IBD is a chronic relapsing-remitting disease in which histological evidence of epithelial healing is critical for long-term remission (45, 46). Current therapy is mainly focused on reducing the inflammatory response; however, proper healing of the mucosal epithelial barrier is essential to long-term remission and requires effective energy metabolism.

Materials and Methods

Mice. Eight- to 10-week-old C57BL/6J were purchased from the Jackson Laboratory. ENU mutagenesis was performed as previously described (47). Mutagenized G0 males were bred to C57BL/6J females, and the resulting G1

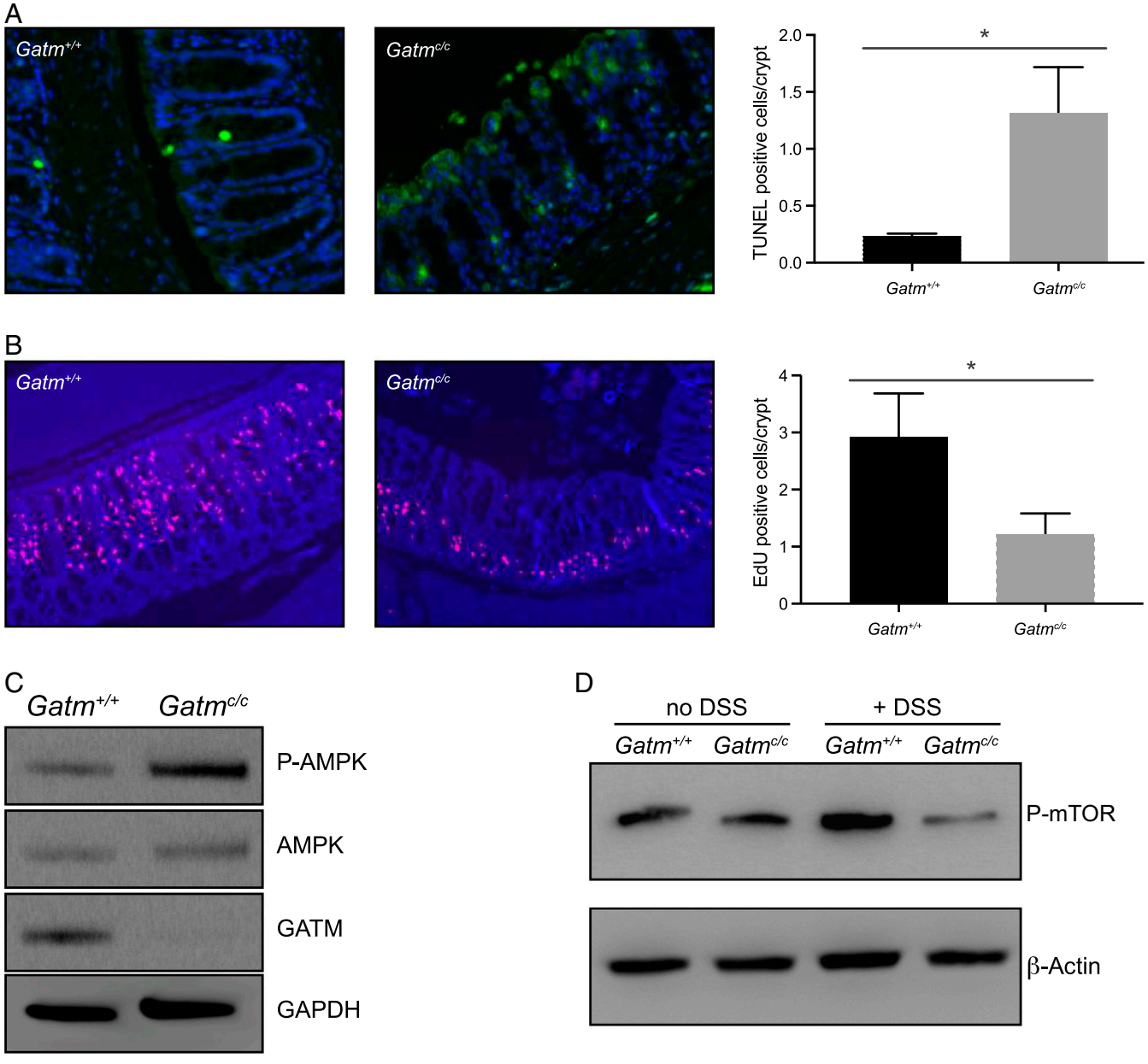

Fig. 5. Colonic epithelium of *Gatm*$^{c/c}$ mice exhibit reduced proliferation and increased cell death during DSS treatment. (*A*) Images of TUNEL staining (green) of colon sections from *Gatm*$^{+/+}$ and *Gatm*$^{c/c}$ mice on day 4 of 1.5% DSS treatment (20× magnification); images are representative of three independent experiments. Quantification was performed on a minimum of 50 crypts for *Gatm*$^{+/+}$ ($n = 3$) and *Gatm*$^{c/c}$ ($n = 3$) colons. *$P < 0.05$. (*B*) Metabolic labeling of DNA in *Gatm*$^{+/+}$ and *Gatm*$^{c/c}$ colons on day 4 of 1.5% DSS treatment. EdU-labeled DNA was stained with Click-iT EdU labeling Alexa Fluor 647 (20× magnification); images are representative of at least three independent experiments. Quantification was performed on a minimum of 50 crypts for *Gatm*$^{+/+}$ ($n = 5$) and *Gatm*$^{c/c}$ ($n = 5$) colons. *$P < 0.05$. (*C* and *D*) Colonic epithelium extracts were assessed by Western blot on day 4 of 1.5% DSS treatment for phosphorylated AMPK (*C*) and phosphorylated mTOR (*D*). Results are representative of more than three independent experiments with at least three mice per group. (*A* and *B*) *P* values were calculated by Student's *t* test; bars indicate mean ± SD.

males were crossed to C57BL/6J females to produce G2 mice. G2 females were backcrossed to their G1 sires to yield G3 mice, which were screened for phenotypes. For the DSS-induced colitis screen, mice received 1.5% DSS (MP Biomedicals) in the drinking water for 7 d followed by an additional 3 d off DSS. Weight was recorded daily and reported as the amount of weight loss from the pretreatment weight. Stool score is a composite score of stool bleeding and constancy determined as previously described (38). Stool consistency: 0 (normal), 2 (loose stool), and 4 (diarrhea); and bleeding: 0 (no blood), 1 (hemoccult positive), 2 (hemoccult positive and visual pellet bleeding), and 4 (gross bleeding, blood around anus). All mice were housed in the University of Texas Southwestern vivarium. All experiments in this study were approved by the University of Texas Southwestern Medical Center Institutional Animal Care and Use Committee, and were performed in accordance with institutionally approved protocols.

Generation of the *Gatm*$^{c/c}$ Mouse Strain Using the CRISPR/Cas9 System. To generate the *Gatm*$^{c/c}$ mouse strain, female C57BL/6J mice were superovulated by injection of 6.5 U pregnant mare serum gonadotropin (Millipore), followed by injection of 6.5 U human chorionic gonadotropin (Sigma-Aldrich) 48 h later. The superovulated mice were subsequently mated overnight with C57BL/6J male mice. The following day, fertilized eggs were collected from the oviducts and in vitro-transcribed Cas9 mRNA (50 ng/μL) and *Gatm* small base-pairing guide RNA (50 ng/μL; 5′-GGCCACCCATCCTCTGCCCA-3′) were injected into the cytoplasm or pronucleus of the embryos. The injected embryos were cultured in M16 medium (Sigma-Aldrich) at 37 °C in 5% CO_2. For the production of mutant mice, two-cell-stage embryos were transferred into the ampulla of the oviduct (10–20 embryos per oviduct) of pseudopregnant Hsd:ICR (CD-1) female mice (Harlan Laboratories).

Sequencing and Determination of Candidate Genes. Whole-exome sequencing and mapping were performed as described (48). Briefly, exome-enriched DNA from all G1 mice was sequenced using the Illumina HiSeq 2500 platform. All G3 mice were genotyped across coding mutations according to their pedigree using Ion Torrent AmpliSeq custom panels as previously described (48). To correlate mice with the genotyping results, we used the percentage of original weight loss as a continuous variable.

Crypt Isolation. Colonic crypts were isolated as previously described (6). Briefly, colons were isolated from mice and stool removed from the lumen. Colons were then cut to 5- to 10-mm pieces and incubated at room temperature for 30 min in PBS containing 5 mM EDTA.

Antibodies. Antibodies for Western blot: GATM (Sigma), AMPK, p-mTOR, p-AMPK, β-actin, and GAPDH (Cell Signaling Technologies).

Histology and Microscopy. Freshly isolated colons were fixed in formalin and embedded in paraffin. Hematoxylin–eosin staining was conducted using a standard protocol by the University of Texas Southwestern Histology core. TUNEL staining was done using the TdT In Situ Apoptosis Detection Kit per manufacturer's instruction (R&D Systems). EdU DNA labeling was performed by injecting mice intraperitoneally with 1 mg/kg of EdU (Invitrogen) in PBS. After 4 h, distal colonic tissue was fixed and embedded in paraffin. EdU staining was performed using a Click-iT EdU labeling kit according to manufacturer's instructions (Invitrogen).

FITC–Dextran Permeability Assay. Intestinal permeability was assessed by administration of FITC–dextran 4000 (Sigma). After a 4-h fast, mice were orally gavaged with FITC–dextran (20 mg/100 g body weight). Whole blood was obtained by cheek bleeding, and fluorescence was measured in the serum by a fluorometer (BioTek) at 488 nm.

Quantitative RT-PCR. Total RNA from colonic epithelium was isolated using TRIzol reagent (Thermo Fisher) according to the manufacturer's instructions. DNase treatment and cleanup was performed with the DNA-free DNase Treatment and Removal Reagents kit (Thermo Fisher). The isolated RNA was subsequently purified on a silica column (Invitrogen) to remove any excess DSS, which can interfere with the reverse-transcriptase reaction. One microgram of RNA was reverse-transcribed to cDNA with SuperScript III First-Strand Synthesis System for RT-PCR (Life Technologies). Transcript levels of *Cxcl2*, *Il6*, and *Tnf* were analyzed using iTaq Universal SYBR Green Supermix (Bio-Rad) on a Step One Plus Real-Time PCR System (Life Technologies) with the following primers: *Cxcl2*: 5′-GCTTCCTCCTTCCTTCTGGT-3′, 5′-GGGCAGAAAGCTTGTCTCAA-3′; *Il6:* 5-GTCAGGGGTGGTTATTGCAT-3′, 5′-AGTGAGGAACAAGCCAGAGC-3′; *Tnf*: 5′-AGATGATCTGACTGCCTGGG-3′, 5′-CTGCTGCACTTTGGAGTGAT-3′. Relative expression was calculated using the ΔΔCt standardization method using *Actb* (5′-GTTGTCGACGACGAGCG-3′ and 5′-GCACAGAGCCTCCGCCTT-3′).

Flow Cytometry. Blood cells were isolated and incubated as previously described (48). Data were acquired on a LSRFortessa cell analyzer (BD Biosciences) and analyzed with FlowJo software (TreeStar). Cell sorting was performed on a FACSAria II cell sorter (BD Biosciences).

Creatine Concentration Assay. Epithelial cells were isolated as above. Cell suspension was lysed and sonicated in a creatine assay buffer (Sigma) and then passed through a 10-kD molecular mass cutoff spin column (Amicon) to remove high molecular-mass proteins. Creatine concentration was assessed using a creatine concentration assay (Sigma) per manufacturer's guidelines.

Trinitrobenzene Sulfonic Acid Colitis. Induction of trinitrobenzene sulfonic acid (TNBS) colitis has been previously described. Briefly, 5-mo-old male *Gatm*$^{+/+}$, *Gatm*$^{c/+}$, and *Gatm*$^{c/c}$ mice were anesthetized using isoflurane and then administered 3 mg TNBS (Sigma) intrarectally in 50% ethanol solution. Mice were held vertically for 60 s to allow for retention of the TNBS enema. Mice were euthanized on day 4 and colons harvested for analysis.

Mitochondrial Mass. *Gatm*$^{+/+}$ and *Gatm*$^{c/c}$ mice were administered 1.5% DSS for 3 d and colonocytes harvested. Cells were incubated in 40 nM MitoTracker Green (Life Technologies) for 15 min at 37 °C. Single cells were washed with PBS and data acquired with a LSRFortessa cell analyzer (BD Biosciences) and analyzed with FlowJo software (TreeStar).

Mitochondrial Stress Test. *Gatm*$^{+/+}$ and *Gatm*$^{c/c}$ mice were administered 1.5% DSS for 3 d. On day 3, colonic crypts were harvested as described above. The oxygen consumption rate was measured using an XF-24 Extracellular Flux Analyzer (Seahorse Bioscience). Basal oxygen consumption was assessed before the addition of any mitochondrial inhibitor. ATP production, maximal respiration, and spare capacity were determined using an XF cell mitochondrial stress test (Seahorse Bioscience) per manufacturer guidelines.

Statistical Analysis. Statistical analysis was performed using GraphPad Prism software and Student's *t* test. All differences with $P < 0.05$ were considered significant. *P* values are denoted by $*P < 0.05$, $**P < 0.01$, and $***P < 0.001$; not significant with $P > 0.05$.

ACKNOWLEDGMENTS. We thank Katherine Timer for expert assistance with figure preparation. This work was supported by Crohn's & Colitis Foundation of America Fellowship Award 2014CCFA00RFA0000090037 (to E.T.); NIH K08 Grant DK107886 (to E.T.); Immunology T32 Training Grant AI005184 (to W.M.), and NIH Grant R37 GM066759 (to B.B.).

1. Cho JH, Gregersen PK (2011) Genomics and the multifactorial nature of human autoimmune disease. *N Engl J Med* 365(17):1612–1623.
2. Cardinale CJ, Kelsen JR, Baldassano RN, Hakonarson H (2013) Impact of exome sequencing in inflammatory bowel disease. *World J Gastroenterol* 19(40):6721–6729.
3. Abraham C, Cho JH (2009) Inflammatory bowel disease. *N Engl J Med* 361(21): 2066–2078.
4. Brandl K, Beutler B (2012) Creating diseases to understand what prevents them: Genetic analysis of inflammation in the gastrointestinal tract. *Curr Opin Immunol* 24(6):678–685.
5. Brandl K, et al. (2009) Enhanced sensitivity to DSS colitis caused by a hypomorphic Mbtps1 mutation disrupting the ATF6-driven unfolded protein response. *Proc Natl Acad Sci USA* 106(9):3300–3305.
6. Brandl K, Tomisato W, Beutler B (2012) Inflammatory bowel disease and ADAM17 deletion. *N Engl J Med* 366(2):190, author reply 190.
7. Brandl K, et al. (2012) Yip1 domain family, member 6 (Yipf6) mutation induces spontaneous intestinal inflammation in mice. *Proc Natl Acad Sci USA* 109(31):12650–12655.
8. Shah YM, et al. (2008) Hypoxia-inducible factor augments experimental colitis through an MIF-dependent inflammatory signaling cascade. *Gastroenterology* 134(7): 2036–2048, 2048.e2031–2033.
9. Adzhubei IA, et al. (2010) A method and server for predicting damaging missense mutations. *Nat Methods* 7(4):248–249.
10. Barry ER, et al. (2013) Restriction of intestinal stem cell expansion and the regenerative response by YAP. *Nature* 493(7430):106–110.
11. Bertolotti A, et al. (2001) Increased sensitivity to dextran sodium sulfate colitis in IRE1beta-deficient mice. *J Clin Invest* 107(5):585–593.
12. McConnell BB, et al. (2011) Kruppel-like factor 5 protects against dextran sulfate sodium-induced colonic injury in mice by promoting epithelial repair. *Gastroenterology* 140(2): 540–549.e542.

13. Alangari A, et al. (2012) LPS-responsive beige-like anchor (LRBA) gene mutation in a family with inflammatory bowel disease and combined immunodeficiency. *J Allergy Clin Immunol* 130(2):481–8.e482.
14. Alkhairy OK, et al. (2016) Spectrum of phenotypes associated with mutations in LRBA. *J Clin Immunol* 36(1):33–45.
15. Serwas NK, et al. (2015) Atypical manifestation of LRBA deficiency with predominant IBD-like phenotype. *Inflamm Bowel Dis* 21(1):40–47.
16. Humm A, Fritsche E, Steinbacher S, Huber R (1997) Crystal structure and mechanism of human L-arginine:glycine amidinotransferase: A mitochondrial enzyme involved in creatine biosynthesis. *EMBO J* 16(12):3373–3385.
17. Choe CU, et al. (2013) L-arginine:glycine amidinotransferase deficiency protects from metabolic syndrome. *Hum Mol Genet* 22(1):110–123.
18. Zhang Y, Li H, Wang X, Gao X, Liu X (2009) Regulation of T cell development and activation by creatine kinase B. *PLoS One* 4(4):e5000.
19. Beal MF (2011) Neuroprotective effects of creatine. *Amino Acids* 40(5):1305–1313.
20. Klivenyi P, et al. (1999) Neuroprotective effects of creatine in a transgenic animal model of amyotrophic lateral sclerosis. *Nat Med* 5(3):347–350.
21. Mooney SM, et al. (2011) Creatine kinase brain overexpression protects colorectal cells from various metabolic and non-metabolic stresses. *J Cell Biochem* 112(4): 1066–1075.
22. Stockebrand M, Sauter K, Neu A, Isbrandt D, Choe CU (2013) Differential regulation of AMPK activation in leptin- and creatine-deficient mice. *FASEB J* 27(10):4147–4156.
23. Song X, et al. (2014) Role of AMP-activated protein kinase in cross-talk between apoptosis and autophagy in human colon cancer. *Cell Death Dis* 5:e1504.
24. Guan Y, et al. (2015) Repression of mammalian target of rapamycin complex 1 inhibits intestinal regeneration in acute inflammatory bowel disease models. *J Immunol* 195(1):339–346.
25. Sampson LL, Davis AK, Grogg MW, Zheng Y (2016) mTOR disruption causes intestinal epithelial cell defects and intestinal atrophy postinjury in mice. *FASEB J* 30(3): 1263–1275.
26. Holland WL, et al. (2007) Inhibition of ceramide synthesis ameliorates glucocorticoid-, saturated-fat-, and obesity-induced insulin resistance. *Cell Metab* 5(3):167–179.
27. Omae F, Miyazaki M, Enomoto A, Suzuki A (2004) Identification of an essential sequence for dihydroceramide C-4 hydroxylase activity of mouse DES2. *FEBS Lett* 576(1-2):63–67.
28. Omae F, et al. (2004) DES2 protein is responsible for phytoceramide biosynthesis in the mouse small intestine. *Biochem J* 379(Pt 3):687–695.
29. Christian BE, Spremulli LL (2009) Evidence for an active role of IF3mt in the initiation of translation in mammalian mitochondria. *Biochemistry* 48(15):3269–3278.
30. van der Sluis R, et al. (2015) Conservation of the coding regions of the glycine N-acyltransferase gene further suggests that glycine conjugation is an essential detoxification pathway. *Gene* 571(1):126–134.
31. Wang S, et al. (2007) Cloning and functional characterization of a novel mitochondrial N-ethylmaleimide-sensitive glycerol-3-phosphate acyltransferase (GPAT2). *Arch Biochem Biophys* 465(2):347–358.
32. Colgan SP, Curtis VF, Campbell EL (2013) The inflammatory tissue microenvironment in IBD. *Inflamm Bowel Dis* 19(10):2238–2244.
33. Glover LE, Colgan SP (2011) Hypoxia and metabolic factors that influence inflammatory bowel disease pathogenesis. *Gastroenterology* 140(6):1748–1755.
34. Kominsky DJ, Campbell EL, Colgan SP (2010) Metabolic shifts in immunity and inflammation. *J Immunol* 184(8):4062–4068.
35. Glover LE, et al. (2013) Control of creatine metabolism by HIF is an endogenous mechanism of barrier regulation in colitis. *Proc Natl Acad Sci USA* 110(49): 19820–19825.
36. Jostins L, et al.; International IBD Genetics Consortium (IIBDGC) (2012) Host-microbe interactions have shaped the genetic architecture of inflammatory bowel disease. *Nature* 491(7422):119–124.
37. Wyss M, Kaddurah-Daouk R (2000) Creatine and creatinine metabolism. *Physiol Rev* 80(3):1107–1213.
38. Su RY, Chao Y, Chen TY, Huang DY, Lin WW (2007) 5-Aminoimidazole-4-carboxamide riboside sensitizes TRAIL- and TNFalpha-induced cytotoxicity in colon cancer cells through AMP-activated protein kinase signaling. *Mol Cancer Ther* 6(5):1562–1571.
39. Mihaylova MM, Shaw RJ (2011) The AMPK signalling pathway coordinates cell growth, autophagy and metabolism. *Nat Cell Biol* 13(9):1016–1023.
40. Huo HZ, et al. (2013) AMP-activated protein kinase (AMPK)/Ulk1-dependent autophagic pathway contributes to C6 ceramide-induced cytotoxic effects in cultured colorectal cancer HT-29 cells. *Mol Cell Biochem* 378(1-2):171–181.
41. Dzamko N, et al. (2010) AMPK beta1 deletion reduces appetite, preventing obesity and hepatic insulin resistance. *J Biol Chem* 285(1):115–122.
42. O'Neill HM, et al. (2011) AMP-activated protein kinase (AMPK) beta1beta2 muscle null mice reveal an essential role for AMPK in maintaining mitochondrial content and glucose uptake during exercise. *Proc Natl Acad Sci USA* 108(38):16092–16097.
43. O'Neill LA, Hardie DG (2013) Metabolism of inflammation limited by AMPK and pseudo-starvation. *Nature* 493(7432):346–355.
44. Vieira RP, et al. (2007) Creatine supplementation exacerbates allergic lung inflammation and airway remodeling in mice. *Am J Respir Cell Mol Biol* 37(6):660–667.
45. Villanacci V, Antonelli E, Geboes K, Casella G, Bassotti G (2013) Histological healing in inflammatory bowel disease: A still unfulfilled promise. *World J Gastroenterol* 19(7): 968–978.
46. Cohen RD (2010) The pharmacoeconomics of biologic therapy for IBD. *Nat Rev Gastroenterol Hepatol* 7(2):103–109.
47. Georgel P, Du X, Hoebe K, Beutler B (2008) ENU mutagenesis in mice. *Methods Mol Biol* 415:1–16.
48. Wang T, et al. (2015) Real-time resolution of point mutations that cause phenovariance in mice. *Proc Natl Acad Sci USA* 112(5):E440–E449.

Supporting Information

Turer et al. 10.1073/pnas.1621400114

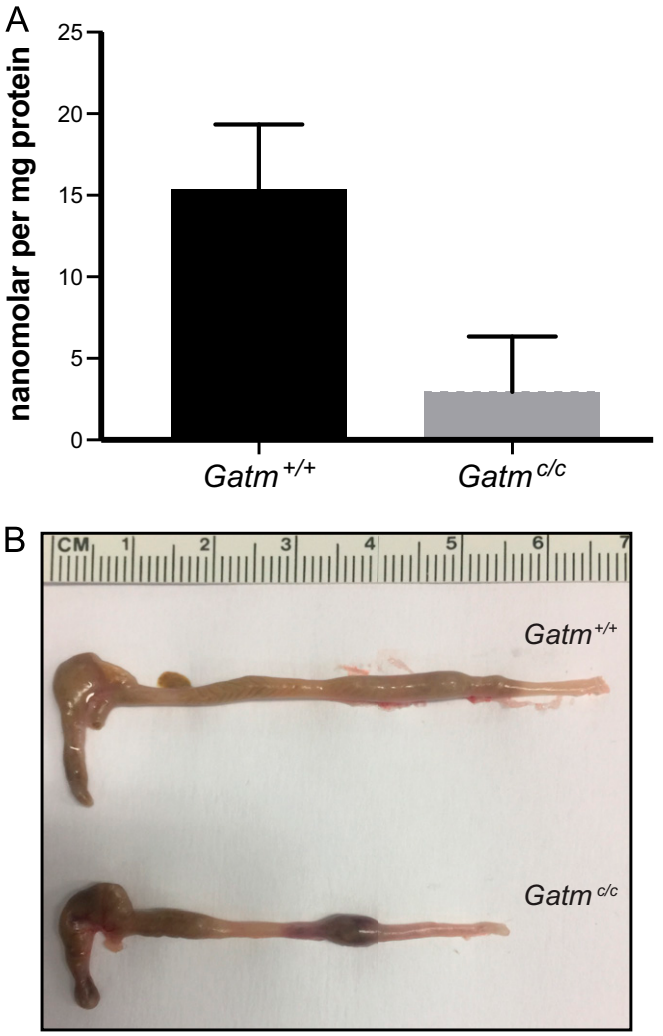

Fig. S1. Creatine content and colitis induced shortening of *Gatm*$^{c/c}$ colons. (*A*) Creatine concentration in *Gatm*$^{c/c}$ ($n = 4$) and littermate control (*Gatm*$^{+/+}$, $n = 4$) colonic epithelial cells. $P < 0.005$. (*B*) Colons of *Gatm*$^{c/c}$ mice exposed to 1.4% DSS for 8 d exhibited shortening. Representative colons are shown for each genotype.

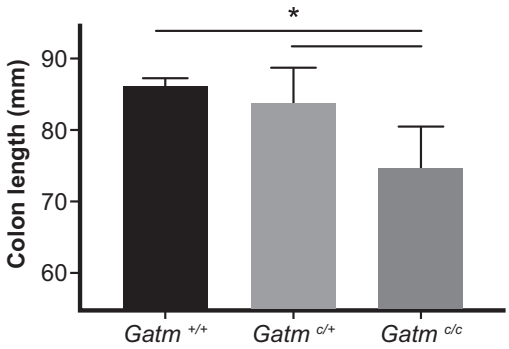

Fig. S2. Colons of trinitrobenzenesulfonic acid (TNBS)-treated *Gatm*$^{c/c}$ mice. Colons of *Gatm*$^{c/c}$ displayed shortening postintrarectal administration of TNBS. Five-month-old male *Gatm*$^{+/+}$ ($n = 4$), *Gatm*$^{c/+}$ ($n = 5$), and *Gatm*$^{c/c}$ ($n = 5$) mice were administered 3 mg of TNBS intrarectally, and colons were harvested and measured 4 d posttreatment. *$P < 0.05$; determined by Student's t test.

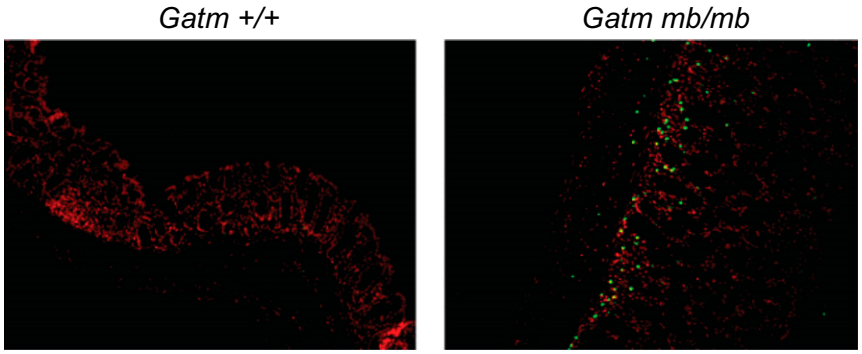

Fig. S3. TUNEL staining of *Gatm*$^{mb/mb}$ colons. Images of TUNEL staining (green) of colon sections from *Gatm*$^{+/+}$ and *Gatm*$^{mb/mb}$ mice on day 6 of 1.5% DSS treatment (10× magnification); images are representative of three independent experiments.

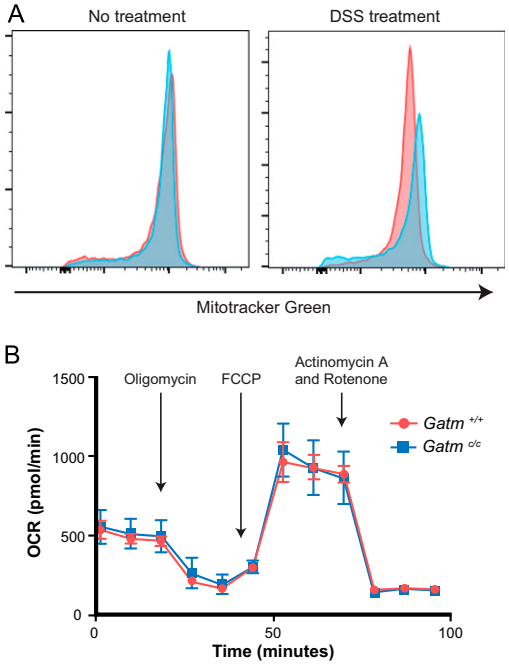

Fig. S4. Mitochondrial mass and functioning in *Gatm*$^{c/c}$ colonocytes. (*A*) Colonocytes from untreated and 3 d DSS-treated *Gatm*$^{c/c}$ (blue) vs. *Gatm*$^{+/+}$ littermates (red) were harvested and stained with MitoTracker Green. Data are representative of three independent experiments. (*B*) Mitochondrial respiration of colonic crypts from mice of the indicated genotypes treated for 3 d with 1.5% DSS was tested using Seahorse Flux. Oligomycin, carbonyl cyanide 4-(trifluoromethoxy) phenylhydrazone (FCCP), and a mix of rotenone and antimycin A were serially injected to measure ATP-linked respiration, maximal respiration, and non-mitochondrial respiration, respectively. Data are representative of three independent experiments.